

Tunable Noise Cross Correlations in a Double Quantum Dot

D. T. McClure, L. DiCarlo, Y. Zhang, H.-A. Engel, and C. M. Marcus
Department of Physics, Harvard University, Cambridge, Massachusetts 02138, USA

M. P. Hanson and A. C. Gossard

Department of Materials, University of California, Santa Barbara, California 93106, USA

(Received 11 July 2006; published 29 January 2007)

We report measurements of the cross correlation between temporal current fluctuations in two capacitively coupled quantum dots in the Coulomb blockade regime. The sign of the cross-spectral density is found to be tunable by gate voltage and source-drain bias. We find good agreement with the data by including an interdot Coulomb interaction in a sequential-tunneling model.

DOI: [10.1103/PhysRevLett.98.056801](https://doi.org/10.1103/PhysRevLett.98.056801)

PACS numbers: 73.50.Td, 05.40.Ca, 73.23.Hk, 73.63.Kv

Current noise cross correlation in mesoscopic electronics, the fermionic counterpart of intensity-intensity correlation in quantum optics, is sensitive to quantum indistinguishability as well as many-body interactions [1–5]. A distinctive feature of fermionic systems is that in the absence of interactions, noise cross correlation is expected to always be negative [6]. Experimentally, negative correlations have been observed in several solid-state Hanbury Brown–Twiss–type noise measurements [7–9]. Since no sign constraint exists for interacting systems, a positive noise cross correlation in a Fermi system is a characteristic signature of interactions.

Sign reversal of noise cross correlation has been the focus of recent theory and experiment [10–18]. Theory indicates that positive cross correlations can arise in the presence of BCS-like interaction [10], dynamical screening [11,12], dynamical channel blockade [13], and strong inelastic scattering [12,14–16]. Experimentally, sign reversal of noise cross correlation has been realized using a voltage probe to induce inelastic scattering [17], and in a beam-splitter geometry, where the sign reversal was linked to a crossover from sub- to super-Poissonian noise in a tunnel-barrier source [18]. This crossover was attributed to Coulomb interaction between naturally occurring localized states in the tunnel barrier [19], as has been done in experiments on GaAs MESFETs [20] and stacked, self-assembled quantum dots [21].

In this Letter, we investigate gate-controlled sign reversal of noise cross correlation in a simple four-terminal device. The structure consists of a parallel, capacitively coupled double quantum dot operated in the Coulomb blockade regime. In this configuration, the double dot acts as a pair of tunable interacting localized states, enabling a systematic study of Coulomb-induced correlation. Turning off interdot tunneling by electrically depleting the connection between dots ensures that indistinguishability (i.e., Fermi statistics) alone cannot induce any cross correlation; any cross correlation, positive or negative, requires interdot Coulomb interaction. We find good agreement

between the experimental results and a sequential-tunneling model of capacitively coupled single-level dots.

The four-terminal double-dot device [see Fig. 1(a)] is defined by top gates on a GaAs/Al_{0.3}Ga_{0.7}As heterostructure grown by molecular beam epitaxy. The two-

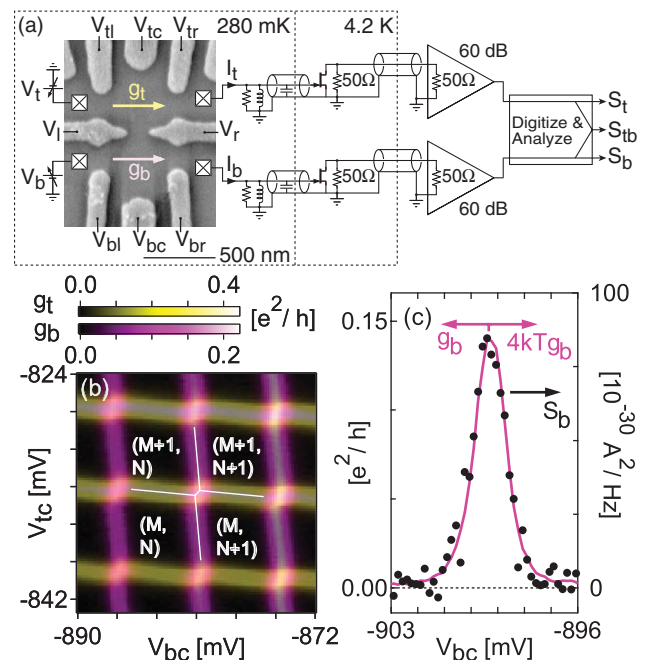


FIG. 1 (color). (a) Scanning electron micrograph of the double-dot device, and equivalent circuit at 2 MHz of the noise detection system measuring the power spectral densities and cross-spectral density of fluctuations in currents I_t and I_b . (b) Differential conductances g_t (yellow) and g_b (magenta) as a function of V_{tc} and V_{bc} over a few Coulomb blockade peaks in each dot, at $V_t = V_b = 0$. Black regions correspond to well-defined charge states in the double-dot system. Superimposed white lines indicate the honeycomb structure resulting from the finite interdot capacitive coupling. (c) Zero-bias (thermal) noise S_b (black dots, right axis), conductance g_b (magenta curve, left axis), and calculated $4k_B T_e g_b$ (magenta curve, right axis) as a function of gate voltage V_{bc} , with $V_{tc} = -852.2$ mV.

dimensional electron gas 100 nm below the surface has density $2 \times 10^{11} \text{ cm}^{-2}$ and mobility $2 \times 10^5 \text{ cm}^2/\text{Vs}$. Gate voltages $V_l = V_r = -1420 \text{ mV}$ fully deplete the central point contact, preventing interdot tunneling. Gate voltages V_{tl} (V_{bl}) and V_{tr} (V_{br}) control the tunnel barrier between the top (bottom) dot and its left and right leads. Plunger gate voltage V_{tc} (V_{bc}) controls the electron number M (N) in the top (bottom) dot; for this experiment $M \sim N \sim 100$. The lithographic area of each dot is $0.15 \mu\text{m}^2$. We estimate level spacing $\Delta_{t(b)} \approx 70 \mu\text{eV}$ in each dot, for $\sim 100 \text{ nm}$ depletion around the gates.

Measurements are performed in a ^3He cryostat using a two-channel noise measurement system [Fig. 1(a)] [22]. A voltage bias V_t (V_b) is applied to the left lead of the top (bottom) dot, with right leads grounded. Separate resistor-inductor-capacitor resonators ($R = 5 \text{ k}\Omega$, $L = 66 \mu\text{H}$, $C = 96 \text{ pF}$) convert fluctuations in currents I_t and I_b through the top and bottom dots around 2 MHz into voltage fluctuations on gates of high electron mobility transistors at 4.2 K, which in turn produce current fluctuations in two 50Ω coaxial lines extending to room temperature, where further amplification is performed. These signals are then simultaneously digitized at 10 MHz, their fast Fourier transforms calculated, and the current noise power spectral densities S_t , S_b and cross-spectral density S_{tb} extracted following 15 s of integration, except for the data in Fig. 1(c), which was averaged for 50 s per point. The total gain of each amplification line and the base electron temperature $T_e = 280 \text{ mK}$ are calibrated *in situ* using Johnson-noise thermometry at base temperature and 1.6 K with the device configured as two point contacts [22]. Differential conductance g_t (g_b) through the top (bottom) dot is measured using standard lock-in techniques with an excitation of 25 (30) μV_{rms} at 677 (1000) Hz. Ohmic contact resistances of roughly a few k Ω , much less than the dot resistances, are not subtracted.

Superposed top- and bottom-dot conductances g_t and g_b as a function of plunger voltages V_{tc} and V_{bc} form the characteristic double-dot honeycomb pattern [23,24], with dark regions corresponding to well-defined electron number in each dot, denoted (M , N) (first index for top dot), as shown in Fig. 1(b). Horizontal (vertical) features in g_t (g_b) are Coulomb blockade (CB) conductance peaks [25], across which M (N) increases by one as V_{tc} (V_{bc}) is raised. The distance between triple points, i.e., the length of the short edge of the hexagon, provides a measure of the mutual charging energy U due to interdot capacitive coupling. By comparing this distance to the CB peak spacing, and using the single-dot charging energy $E_C = 600 \mu\text{eV}$ extracted from finite-bias CB diamonds (not shown), we estimate $U \approx 60 \mu\text{eV}$ [24]. We refer to the midpoint of the short edge of a hexagon, midway between triple points, as a ‘‘honeycomb vertex.’’ Current noise S_b and conductance g_b , measured simultaneously at zero dc bias, over a CB peak in the bottom dot (with the top dot in a CB valley) are shown in Fig. 1(c). Agreement between the measured S_b

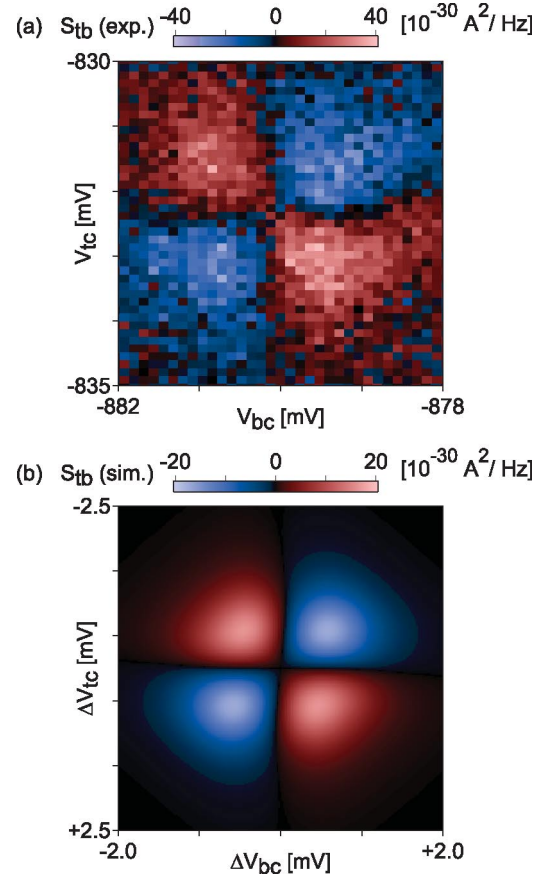


FIG. 2 (color). Measured (a) and simulated (b) cross-spectral density S_{tb} near a honeycomb vertex, with applied bias $V_t = V_b = -100 \mu\text{V}$ ($e|V_{t(b)}| \approx 4k_B T_e \approx E_C/6$). Blue regions (lower-left and upper-right) indicate negative S_{tb} , whereas red regions indicate positive S_{tb} .

and the Johnson-Nyquist thermal noise value $4k_B T_e g_b$ is observed.

Turning now to finite-bias noise measurements, Fig. 2(a) shows the measured cross correlation, S_{tb} , as a function of plunger gate voltages V_{tc} and V_{bc} , in the vicinity of a honeycomb vertex, with voltage bias of $-100 \mu\text{V}$ applied to both dots. The plot reveals a characteristic quadrupole pattern of cross correlation centered on the honeycomb vertex, comprising regions of both negative and positive cross correlation. Similar patterns are observed at all other honeycomb vertices. The precise symmetry of the pattern is found to depend rather sensitively on the relative transparency of each dot’s left and right tunnel barriers. Away from the vertices, noise cross correlation vanishes.

To better understand this experimental result, we model the system as single-level dots capacitively coupled by a mutual charging energy U , each with weak tunneling to the leads. The energy needed to add electron $M + 1$ to the top dot depends on the two plunger gate voltages as well as the electron number $n \in \{N, N + 1\}$ on the bottom dot: $E_t = \alpha_t V_{tc} + \beta_t V_{bc} + U n + \text{const}$, where lever arms α_t and β_t are obtained from the honeycomb plot in Fig. 1(b) [23] and the measured E_C . The energy E_b to add electron $N + 1$ to

the bottom dot is given by an analogous formula. Occupation probabilities for charge states (M, N) , $(M + 1, N)$, $(M, N + 1)$, and $(M + 1, N + 1)$ are given by the diagonal elements of the density matrix, $\rho = (\rho_{00}, \rho_{10}, \rho_{01}, \rho_{11})^T$. The time evolution of ρ is given by a master equation $d\rho/dt = \mathcal{M}\rho$, where

$$\mathcal{M} = \begin{pmatrix} -W_{00}^{\text{out}} & W_{00\leftarrow 10} & W_{00\leftarrow 01} & 0 \\ W_{10\leftarrow 00} & -W_{10}^{\text{out}} & 0 & W_{01\leftarrow 11} \\ W_{01\leftarrow 00} & 0 & -W_{01}^{\text{out}} & W_{10\leftarrow 11} \\ 0 & W_{11\leftarrow 10} & W_{11\leftarrow 01} & -W_{11}^{\text{out}} \end{pmatrix}. \quad (1)$$

Each diagonal term of \mathcal{M} gives the total loss rate for the corresponding state: $W_{\alpha}^{\text{out}} = \sum_{\beta} W_{\beta\leftarrow\alpha}$. Off-diagonal terms give total rates for transitions between two states. For example, $W_{10\leftarrow 00} = W_{10\leftarrow 00}^l + W_{10\leftarrow 00}^r$ is the total tunneling rate into $(M + 1, N)$ from (M, N) , combining contributions from the top-left and top-right leads.

Rates for tunneling between a dot and either of its leads $i \in \{tl, tr, bl, br\}$ depend on both the transparency Γ^i of the tunnel barrier to lead i and the Fermi function $f_i(\epsilon) = [1 + \exp\{(\epsilon - \mu_i)/k_B T_e\}]^{-1}$ evaluated at $\epsilon = E_{t(b)}$, where μ_i is the chemical potential in lead i . For example, the rates for tunneling into and out of the top dot via the left tunnel barrier are given by $W_{10\leftarrow 00}^l = \Gamma^{tl} f_{tl}(E_t)$ and $W_{00\leftarrow 10}^l = \Gamma^{tl} [1 - f_{tl}(E_t)]$, respectively. As E_t is lowered across μ_{tl} , $W_{10\leftarrow 00}^l$ increases from 0 to Γ^{tl} over a range of a few $k_B T_e$, while $W_{00\leftarrow 10}^l$ does the opposite.

We obtain the steady-state value of ρ , denoted $\bar{\rho}$, by solving $\mathcal{M}\bar{\rho} = 0$. Using techniques described in Refs. [26–28], we define current matrices J^{tr} and J^{br} for the top- and bottom-right leads and apply them to $\bar{\rho}$ to obtain average currents $\langle I_{t(b)} \rangle$ and correlator $\langle I_t(\tau) I_b(0) \rangle$ [29]. The cross-spectral density in the low-frequency limit is then given by $S_{tb} = 2 \int_{-\infty}^{\infty} [\langle I_t(\tau) I_b(0) \rangle - \langle I_t \rangle \langle I_b \rangle] d\tau$.

Simulation results for S_{tb} as a function of plunger gate voltages are shown in Fig. 2(b), with all parameters of the model extracted from experiment: $U = 60 \mu\text{eV}$, $T_e = 280 \text{ mK}$, $\Gamma^{tl} = \Gamma^{tr} = 1.5 \times 10^{10} \text{ s}^{-1}$, and $\Gamma^{bl} = \Gamma^{br} = 7.2 \times 10^9 \text{ s}^{-1}$. The Γ^i were estimated from the zero-bias conductance peak height using Eq. 6.3 of Ref. [30], taking left and right barriers equal. The simulation shows the characteristic quadrupole pattern of positive and negative cross correlation, as observed experimentally. We note that the model underestimates S_{tb} by roughly a factor of 2. This may be due to transport processes not accounted for in the model. For instance, elastic cotunneling should be present since the Γ^i are comparable to $k_B T_e / \hbar$. Also, since the voltage-bias energy $e|V_{t(b)}|$ is greater than the level spacing $\Delta_{t(b)}$, transport may occur via multiple levels [13,31,32] and inelastic cotunneling [33–35].

Intuition for how Coulomb interaction in the form of capacitive interdot coupling can lead to the observed noise cross-correlation pattern can be gained by examining energy levels in both dots in the space of plunger gate voltages, as shown in Fig. 3. With both dots tuned near Coulomb blockade peaks, the fluctuations by one in the

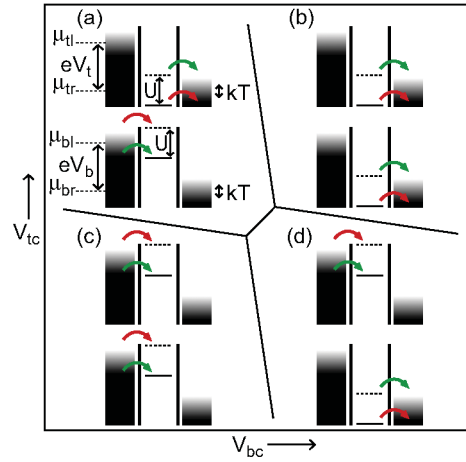


FIG. 3 (color). Energy level diagrams in the vicinity of a honeycomb vertex, with biases $V_{t(b)} = -100 \mu\text{V}$. (The various energies are shown roughly to scale.) The solid horizontal line in the top (bottom) dot represents the energy $E_{t(b)}$ required to add electron $M + 1$ ($N + 1$) when the bottom (top) dot has N (M) electrons. The dashed horizontal line, higher than the solid line by U , represents $E_{t(b)}$ when the bottom (top) dot has $N + 1$ ($M + 1$) electrons. In each dot, the rate of either tunneling in from the left or tunneling out to the right is significantly affected by this difference in the energy level, taking on either a slow value (red arrow) or a fast value (green arrow) depending on the electron number in the other dot. In (a) and (d), where the occurrence of each U -sensitive process enhances the rate of the other, we find positive cross correlation. In (b) and (c), where the occurrence of each U -sensitive process suppresses the rate of the other, we find negative cross correlation.

electron number of each dot, caused by the sequential tunneling of electrons through that dot, cause the energy level of the other dot to fluctuate between two values separated by U . These fluctuations can raise and lower the level across the chemical potential in one of the leads of the dot, strongly affecting either the tunnel-in rate (from the left, for the case illustrated in Fig. 3) or the tunnel-out rate (to the right) of that dot. Specifically, the rate of the “ U -sensitive” process in each dot fluctuates between a slow rate (red arrow), suppressed well below Γ^i , and a fast rate (green arrow), comparable to Γ^i . For balanced right and left Γ^i in each dot, the U -sensitive process becomes the transport bottleneck when its rate is suppressed.

These U -sensitive processes correlate transport through the dots. In region (b) of Fig. 3, for instance, where S_{tb} is negative, the U -sensitive process in each dot is tunneling out. Here and in (c), where the U -sensitive process in each dot is tunneling in, the U -sensitive processes compete: occurrence of one suppresses the other, leading to negative S_{tb} . Conversely, in region (a) [(d)], where S_{tb} is positive, the top [bottom] dot’s U -sensitive process is tunneling out, but the bottom [top] dot’s is tunneling in. Here, the U -sensitive processes cooperate: occurrence of one lifts the suppression of the other, leading to positive S_{tb} .

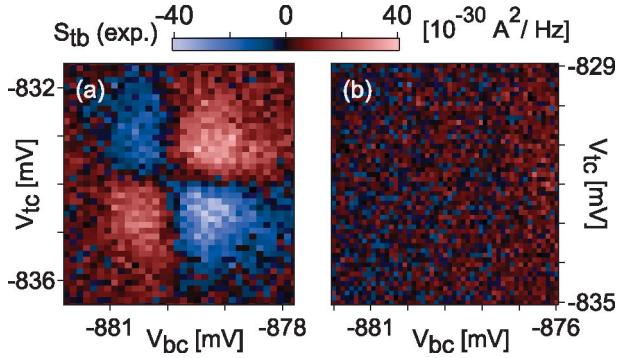


FIG. 4 (color). (a) Measured S_{tb} near a honeycomb vertex, with opposite biases $V_t = -V_b = -100 \mu\text{V}$. Note that the pattern is reversed from Fig. 2(a): negative cross correlation (blue) is now found in the upper-left and lower-right regions, while positive cross correlation (red) is now found in the lower-left and upper-right. (b) Measured S_{tb} near a honeycomb vertex, with $V_t = V_b = 0$. Cross correlation vanishes at zero bias, though the noise in each dot is finite.

The arguments above also apply when one or both biases are reversed. When both are reversed, we find both experimentally and in the model that the same cross-correlation pattern as in Fig. 2 appears (not shown). When only one of the biases is reversed, we find both experimentally [as shown in Fig. 4(a)] and in the model that the pattern reverses sign. In the absence of any bias, cross correlation vanishes both experimentally [as shown in Fig. 4(b)] and in the model, despite the fact that noise in the individual dots remains finite [as seen in Fig. 1(c)].

In conclusion, we have observed gate-controlled sign reversal of noise cross correlation in a double quantum dot in the Coulomb blockade regime with purely capacitive interdot coupling. Experimental observations are in good agreement with a sequential-tunneling model, and can be understood from an intuitive picture of mutual charge-state-dependent tunneling. This study, notable for the simplicity and controllability of the device, may be particularly useful for understanding current noise in systems where interacting localized states occur naturally and uncontrollably.

We thank N. J. Craig for device fabrication and M. Eto, W. Belzig, C. Bruder, E. Sukhorukov, and L. Levitov for valuable discussions. We acknowledge support from the NSF through the Harvard NSEC, PHYS No. 01-17795, No. DMR-05-41988, No. DMR-0501796, as well as support from NSA/DTO and Harvard University.

[1] Ya. M. Blanter and M. Büttiker, Phys. Rep. **336**, 1 (2000); Ya. M. Blanter, cond-mat/0511478.

- [2] T. Martin *et al.*, in *Quantum Noise in Mesoscopic Physics*, edited by Yu. V. Nazarov, NATO Science Series II Vol. 97 (Kluwer, Dordrecht, 2003).
- [3] P. Samuelsson *et al.*, Phys. Rev. Lett. **92**, 026805 (2004).
- [4] C. W. J. Beenakker *et al.*, in *Fundamental Problems in Mesoscopic Physics*, edited by I. V. Lerner, B. L. Altshuler, and Y. Gefen, NATO Science Series II Vol. 154 (Kluwer, Dordrecht, 2004).
- [5] A. V. Lebedev *et al.*, Phys. Rev. B **71**, 045306 (2005).
- [6] M. Büttiker, Phys. Rev. Lett. **65**, 2901 (1990); Phys. Rev. B **46**, 12485 (1992).
- [7] M. Henny *et al.*, Science **284**, 296 (1999).
- [8] W. D. Oliver *et al.*, Science **284**, 299 (1999).
- [9] S. Oberholzer *et al.*, Physica (Amsterdam) **6**, 314E (2000).
- [10] M. P. Anantram and S. Datta, Phys. Rev. B **53**, 16390 (1996); T. Martin, Phys. Lett. A **220**, 137 (1996); J. Torrés and T. Martin, Eur. Phys. J. B **12**, 319 (1999).
- [11] A. M. Martin and M. Büttiker, Phys. Rev. Lett. **84**, 3386 (2000); I. Safi *et al.*, Phys. Rev. Lett. **86**, 4628 (2001); A. Crepieux *et al.*, Phys. Rev. B **67**, 205408 (2003).
- [12] M. Büttiker, in *Quantum Noise in Mesoscopic Physics*, edited by Yu. V. Nazarov, NATO Science Series II Vol. 97 (Kluwer, Dordrecht, 2003).
- [13] A. Cottet *et al.*, Phys. Rev. B **70**, 115315 (2004); Phys. Rev. Lett. **92**, 206801 (2004).
- [14] C. Texier and M. Büttiker, Phys. Rev. B **62**, 7454 (2000).
- [15] S.-T. Wu and S. Yip, Phys. Rev. B **72**, 153101 (2005).
- [16] V. Rychkov and M. Büttiker, Phys. Rev. Lett. **96**, 166806 (2006).
- [17] S. Oberholzer *et al.*, Phys. Rev. Lett. **96**, 046804 (2006).
- [18] Y. Chen and R. A. Webb, Phys. Rev. Lett. **97**, 066604 (2006).
- [19] Y. Chen and R. A. Webb, Phys. Rev. B **73**, 035424 (2006).
- [20] S. S. Safonov *et al.*, Phys. Rev. Lett. **91**, 136801 (2003).
- [21] P. Barthold *et al.*, Phys. Rev. Lett. **96**, 246804 (2006).
- [22] L. DiCarlo *et al.*, Rev. Sci. Instrum. **77**, 073906 (2006).
- [23] W. G. van der Wiel *et al.*, Rev. Mod. Phys. **75**, 1 (2002).
- [24] I. H. Chan *et al.*, Appl. Phys. Lett. **80**, 1818 (2002).
- [25] L. P. Kouwenhoven *et al.*, in *Mesoscopic Electron Transport*, edited by L. L. Sohn, L. P. Kouwenhoven, and G. Schön (Kluwer, Dordrecht, 1997).
- [26] S. Hershfield *et al.*, Phys. Rev. B **47**, 1967 (1993).
- [27] M. Eto *et al.*, Jpn. J. Appl. Phys. **36**, 4004 (1997).
- [28] G. Kiesslich *et al.*, Phys. Rev. B **68**, 125320 (2003).
- [29] Following the approach of Refs. [26–28], we define $J_{mn,m'n'}^{tr} = e\delta_{nn'}(m - m')W_{mn \leftarrow m'n'}^r$ and $J_{mn,m'n'}^{br} = e\delta_{mm'}(n - n')W_{mn \leftarrow m'n'}^r$. The average currents are given by $\langle I_{t(b)} \rangle = \sum_i [J^{(b)r} \bar{\rho}]_i$, and the low-frequency correlator by $\langle I_t(\tau) I_b(0) \rangle = \sum_i [\theta(\tau) J^{tr} e^{\mathcal{M}\tau} J^{br} \bar{\rho} + \theta(-\tau) J^{br} e^{\mathcal{M}\tau} J^{tr} \bar{\rho}]_i$, where θ is the Heaviside step function.
- [30] C. W. J. Beenakker, Phys. Rev. B **44**, 1646 (1991).
- [31] W. Belzig, Phys. Rev. B **71**, 161301(R) (2005).
- [32] S. Gustavsson *et al.*, Phys. Rev. B **74**, 195305 (2006).
- [33] E. V. Sukhorukov *et al.*, Phys. Rev. B **63**, 125315 (2001).
- [34] A. Thielmann *et al.*, Phys. Rev. Lett. **95**, 146806 (2005).
- [35] E. Onac *et al.*, Phys. Rev. Lett. **96**, 026803 (2006).